Optical Engineering

OpticalEngineering.SPIEDigitalLibrary.org

Solid analyte and aqueous solutions sensing based on a flexible terahertz dual-band metamaterial absorber

Xin Yan
Lan-Ju Liang
Xin Ding
Jian-Quan Yao

SPIE.

Xin Yan, Lan-Ju Liang, Xin Ding, Jian-Quan Yao, "Solid analyte and aqueous solutions sensing based on a flexible terahertz dual-band metamaterial absorber," *Opt. Eng.* **56**(2), 027104 (2017), doi: 10.1117/1.OE.56.2.027104.

Solid analyte and aqueous solutions sensing based on a flexible terahertz dual-band metamaterial absorber

Xin Yan,[a,b] Lan-Ju Liang,[a,b,*] Xin Ding,[a] and Jian-Quan Yao[a]
[a]Tianjin University, College of Precision Instrument and Opto-Electronics Engineering, Tianjin, China
[b]Zaozhuang University, School of Opto-Electronic Engineering, Zaozhuang, China

Abstract. A high-sensitivity sensing technique was demonstrated based on a flexible terahertz dual-band metamaterial absorber. The absorber has two perfect absorption peaks, one with a fundamental resonance (f_1) of the structure and another with a high-order resonance (f_2) originating from the interactions of adjacent unit cells. The quality factor (Q) and figure of merit of f_2 are 6 and 14 times larger than that of f_1, respectively. For the solid analyte, the changes in resonance frequency are monitored upon variation of analyte thickness and index; a linear relation between the amplitude absorption with the analyte thickness is achieved for f_2. The sensitivity (S) is 31.2% refractive index units (RIU^{-1}) for f_2 and 13.7% RIU^{-1} for f_1. For the aqueous solutions, the amplitude of absorption decreases linearly with increasing the dielectric constant for the ethanol–water mixture of f_1. These results show that the designed absorber cannot only identify a solid analyte but also characterize aqueous solutions through the frequency shift and amplitude absorption. Therefore, the proposed absorber is promising for future applications in high-sensitivity monitoring biomolecular, chemical, ecological water systems, and aqueous biosystems. [DOI: 10.1117/1.OE.56.2.027104]

Keywords: terahertz; sensor; metamaterial; absorber.

Paper 161817 received Nov. 21, 2016; accepted for publication Jan. 20, 2017; published online Feb. 11, 2017.

1 Introduction

Nondestructive, highly sensitive sensing techniques are desirable in detecting new chemical and biological samples, especially for ecological water systems and aqueous solutions. Detection techniques for new chemical or biological materials have been employed through numerous physical and chemical methods.[1–4] However, such approaches often require adding an appropriate marker, which may cause the sample to be modified before its reaction with materials.[5–9] Therefore, it is necessary to develop the detection techniques for reliable and effective label free testing.

Terahertz (THz) metamaterial sensors have attracted considerable interest as a promising detection tool because of the THz wave characteristics of low photon energy, which can be detected without damage to materials.[10–13] Recently, THz metamaterial sensors have been used in the nondestructive and label-free detection of materials.[14–18] However, the sensitivity of the previously reported metamaterial biosensors is relatively lower due to the radiative and nonradiative loss. Most detection techniques were carried by different shifts in resonance frequency and rarely considered the changes in amplitude resonance. Furthermore, few reports are available on aqueous solution sensing based on THz metamaterials.[19–24]

In this paper, we report a highly sensitive sensing technique for monitoring materials by THz dual-band metamaterial absorber. We propose the absorber based on double-cross metallic lines owing to the symmetry with sixfold rotational symmetry and the sensing capabilities in terms of the change in resonance frequency and the amplitude absorption. There are two strong narrowband absorption peaks of fundamental resonance f_1 and another with a high-order resonance f_2. In addition, the quality factor (Q) and figure of merit (FOM) of f_2 are 6 and 14 times larger than that of f_1, respectively. Most importantly, a linear relation between the amplitude absorption and the analyte thickness was achieved for the resonance f_2. By studying the ethanol–water mixture, we also demonstrated that the amplitude absorption decreased linearly when increasing the dielectric constant for the resonance f_1. Therefore, the proposed THz metamaterial absorber can be applied to identify biomolecular, chemical, and explosive solvent types and to determine the corresponding concentrations.

*Address all correspondence to: Lan-Ju Liang, E-mail: lianglanju123@163.com

2 Sensor Design and Discussion

2.1 *Terahertz Metamaterial Absorber*

The proposed THz flexible absorber is illustrated in Fig. 1(a) and consists of three layers. The top layer includes a double-cross metallic line structure patterned on the flexible polyimide (PI) film with a thickness of 10 μm, and the bottom layer and metallic line structure are 200-nm-thick gold film. The dielectric constant and loss tangent of PI are 3.1 and 0.05, respectively. The thickness of the designed flexible absorber is 10.4 μm. The unit cell of the absorber is shown in Fig. 1(b), and the geometric parameters are $L = 72$ μm, $w = 6$ μm, and $p_x = p_y = 100$ μm. Figure 1(c) shows the simulation absorption spectra of the absorber through CST Microwave Studio. The unite cell boundary conditions with a tetrahedral mesh were used in the frequency domain solver, in which case the wave ports were automatically added in the direction of normal incidence to the substrate. The amplitude of the transmission S21 and the reflection S11 were obtained and the absorption was calculated using $A = 1\text{-}R\text{-}T = 1\text{-}S_{11}^2 - S_{21}^2$, where S_{21} is zero across the entire frequency range due to the metallic ground plane.

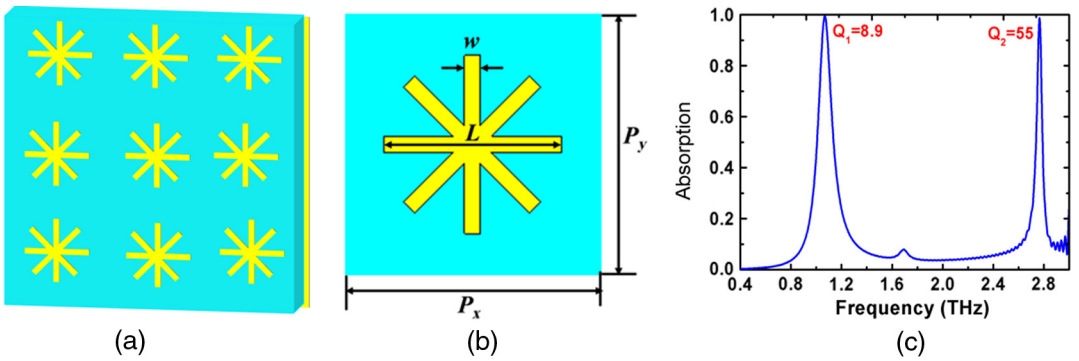

Fig. 1 (a) Structure schematic of the proposed flexible absorber. (b) Unit cell of the absorber, the geometrical parameters are $L = 72$ μm, $w = 6$ μm, and $p_x = p_y = 100$ μm. (c) Simulation absorption spectra of the designed flexible absorber.

The unit cell was subject to the periodic boundary conditions in the x- and y-directions and open for the z-direction in free space. The magnetic and the electric fields were parallel to the x- and y-axes, respectively.

Two distinct absorption peaks are located at around 1.08 (f_1) and 2.77 THz (f_2), with absorptions of over 99.4%. Their qualities Q were 8.9 for f_1 and 55 for f_2 ($Q = f/\text{FWHM}$, where FWHM is the full width at half maximum and f is the frequency of the absorption peak). The Q of resonance f_2 was six times larger than that of the resonance f_1.

Based on the analysis results, the Q characteristics of the resonance f_2 were superior to those of resonance f_1. To understand the physical mechanism of the designed absorber, we simulated the distribution of the electric field ($|E|$) and the magnetic field ($|H_y|$) at the resonances f_2 and f_1 using CST Microwave Studio (Fig. 2). As shown in Figs. 2(a) and 2(b), the electric field for the resonance f_1 was mainly focused on the sides of the metallic array along the direction of the electric field; however, the resonance f_2 was mainly focused on the sides of the metallic array and the area between the units. We also observed that the magnetic field ($|H_y|$) of the resonance f_1 was located on the dielectric layer, but the resonance f_2 was mainly focused on the middle of the unit cell and the area between the units. Consequently, the resonance f_1 was the fundamental resonance of the proposed structure, and the resonance f_2 originated from the interactions of adjacent unit cells as the high-order resonance. Thus, the Q of high-order resonance f_2 was superior to the fundamental resonance f_1. From the simulation analytical results, we also determined that the designed THz dual-band metamaterial absorber was capable of sensing for high-sensitivity monitoring of the materials.

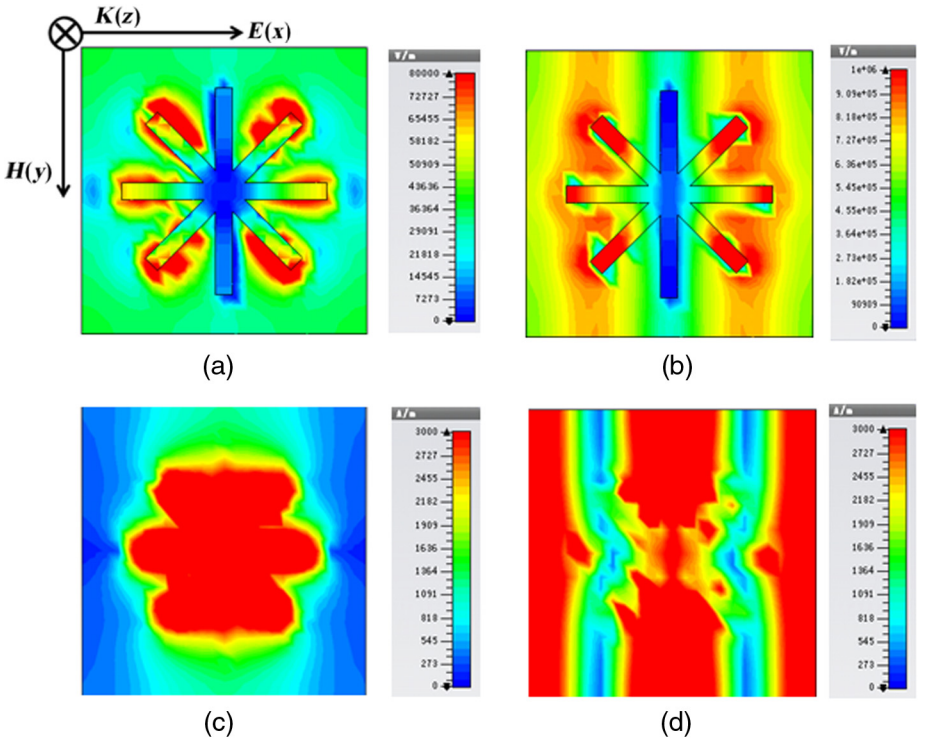

Fig. 2 Distribution of the electric field ($|E|$) for the flexible absorber at the frequencies of (a) 1.07 and (b) 2.77 THz, respectively; distribution of the magnetic field ($|H_y|$) for the flexible absorber at the frequencies of (c) 1.07 and (d) 2.77 THz, respectively.

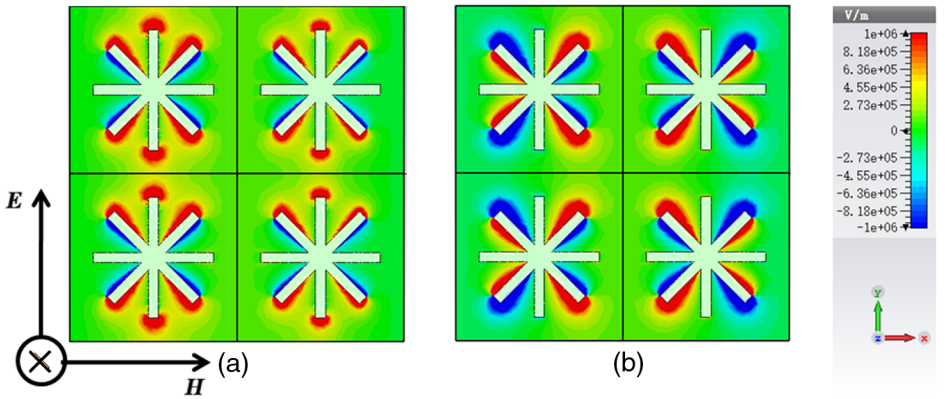

Fig. 3 Distribution of the electric field *E* for the flexible absorber at the frequencies of (a) 1.07 and (b) 1.69 THz, respectively.

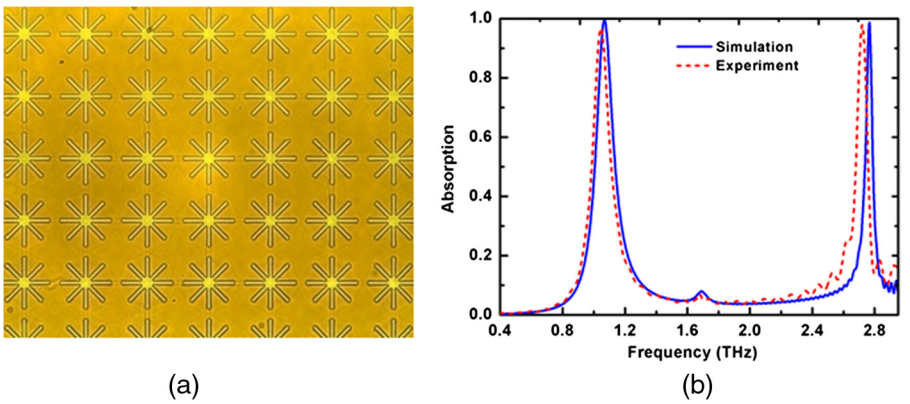

Fig. 4 (a) Microscopic image of a part of the THz flexible absorber and (b) measured and simulated absorption spectra of the THz flexible absorber.

From Fig. 1(c), we also know that there is a third weak peak at about 1.69 THz. In order to explain the physical mechanism of this peak, we numerically simulated the electric field distribution of the resonances 1.07 and 1.69 THz, as shown in Fig. 3. The electric field of 1.07 THz was mainly focused on the sides of the metallic array along the incident electric field. For the resonance 1.56 THz, the electric field was mainly focused on the sides of the cross metal structure, where the angle between the two metal lines' structure and incident electric field direction is 45 deg. Consequently, the third peak at the resonance 1.69 THz originated from the metal line structure as another fundamental resonance.

The designed flexible absorber was fabricated through evaporated, spin-coated, lift-off, and peel-off techniques, and the microscopic image of the absorber was shown in Fig. 4(a). The design absorber was also characterized by THz time-domain spectroscopy using a gold mirror as reference, as shown in Fig. 4(b). There are three absorption peaks at 1.04, 1.67, and 2.73 THz under normal incident angle, and the experimental result agreed with the simulation.

2.2 *Solid Analyte Sensing*

To explore the sensitivity for absorber, PI films of different thicknesses were spin coated on the absorber. The absorber sensor characteristics were simulated using CST Microwave Studio (Fig. 5). From the above analysis, we know that the third peak was relatively weak, so we mainly discuss the sensing characteristics for resonances f_1 and f_1. Figure 5(b) shows the simulated absorption spectra of the absorber under different thicknesses (t) of solid analyte; the red frequency shifts of the resonance f_1 for the film thicknesses 4, 8, and 12 μm were 90, 116, and 134 GHz, respectively. The frequency shifts of 198, 364, and 491 GHz for the 4, 8, and 12 μm thicknesses of the analyte for the resonance f_2 were significantly higher than those of frequency shift f_1. Additionally, the change in the amplitude absorption was apparent with the different thicknesses of the PI film for the resonance f_2.

Figure 5(c) reveals the frequency shifts with solid analyte thickness for the resonance f_1 (dots) and f_2 (stars) with simulated data; the red and blue lines show the exponential fits to the simulation data. The fitting functions are described for the resonance f_1 and f_2, where the total frequency shift saturated at approximately 150.8 and 984.7 GHz, respectively. The fitting functions are described by $y_1 = 982.028 - 984.742e(-\frac{t}{17.243})$ and $y_2 = 160.059 - 150.806e(-\frac{t}{5.893})$, respectively.

From Fig. 5(c), we also noted that the frequency shift became saturated at the analyte thicknesses over 10 and 25 μm of the resonances f_1 and f_2, respectively, and no further significant frequency shift was observed upon increasing the analyte thickness.

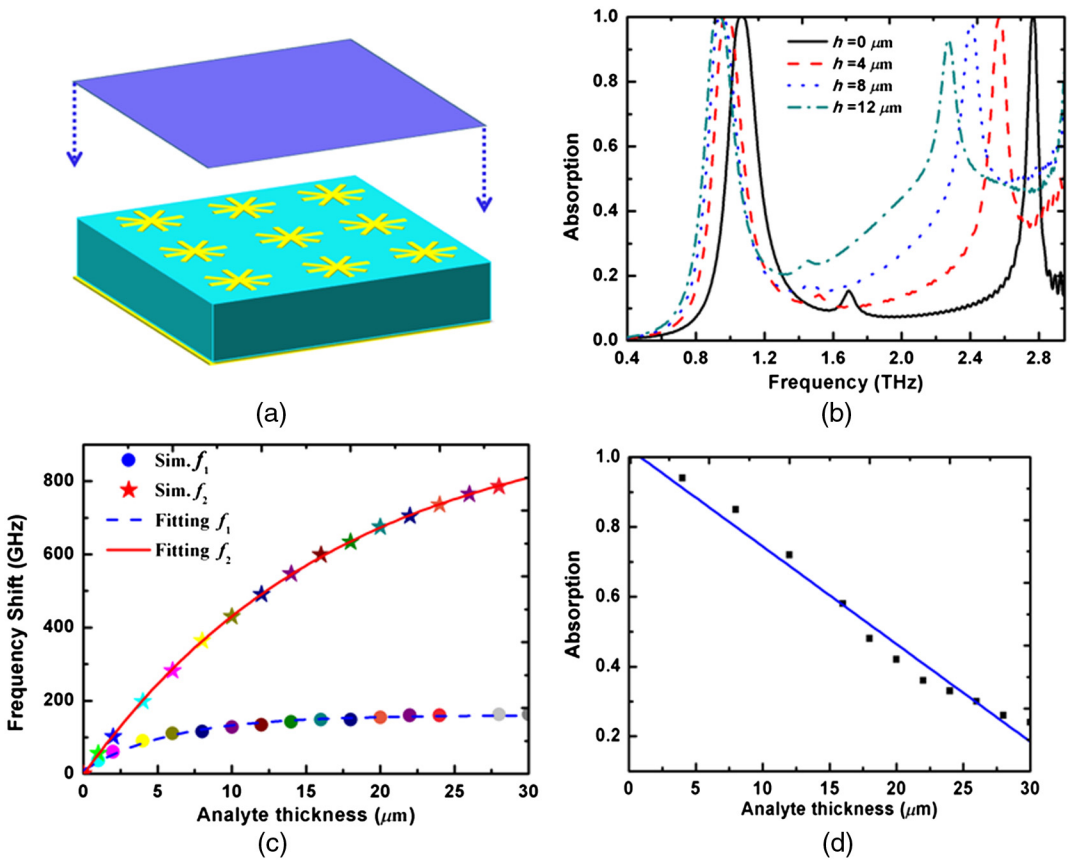

Fig. 5 (a) Diagram of the THz absorber sensor. (b) Simulated absorption spectra of the absorber under different thicknesses of solid analyte. (c) Frequency shift with the analyte thickness for resonance f_1 (dots) and f_2 (stars) with simulated data; the red and blue lines show the exponential fits to the simulation data. (d) Amplitude absorption with solid analyte thickness for resonance f_2.

As shown in Fig. 5(b), the amplitude absorption was different at the film thicknesses 0, 4, 8, and 12 μm for the resonance f_2. The relation between the amplitude absorption with the analyte thickness was also studied as shown in Fig. 5(d); a linear relation can be achieved for the resonance f_2, and the fitting functions are described as $y_3 = 1 - 0.028 * t$ for the resonance f_2. This effect provides an effective method to probe the dielectric properties of the overlayer.

We further characterized the absorber sensor for different refractive indices by CST Microwave Studio under a fixed analyte thickness ($t = 16$ μm) (Fig. 6). Figure 6(a) reveals the simulated absorption spectra of the absorber under different refractive indices. We found the red frequency shifts of the resonances f_1 and f_2 when the refractive index increased from 1.0 to 1.4. The frequency shifts of 0, 200, and 387 GHz for the resonance f_2 were significantly higher than that for resonance f_1. This is due to the higher Q factor of f_1.

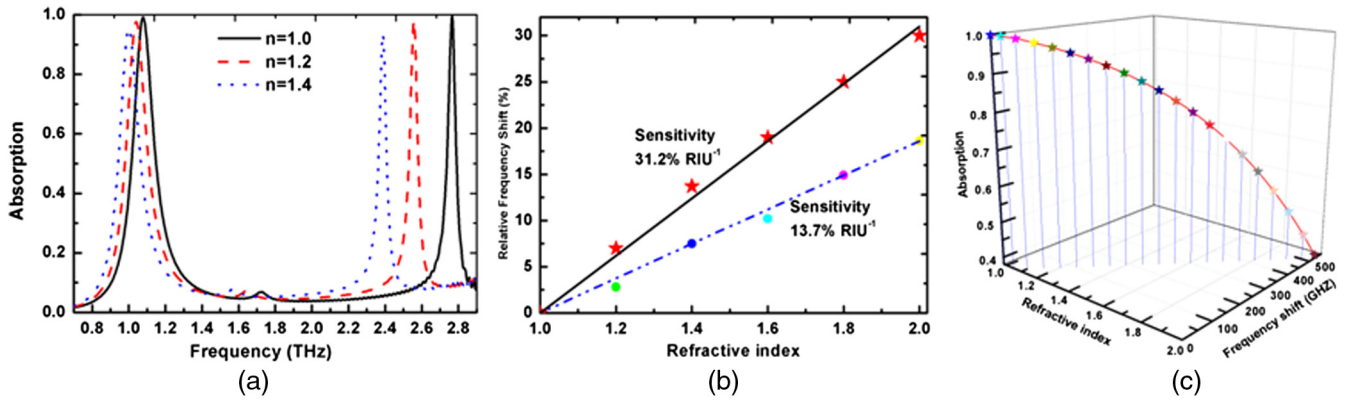

Fig. 6 (a) Simulated absorption spectra of the absorber under different refractive indices. (b) RFS with the refractive index for the resonance f_1 (dots) and f_2 (stars) with simulated data; the red and blue lines show the line fits to the simulation data. (c) Amplitude absorption, frequency shift with the different refractive indices for the resonance f_2.

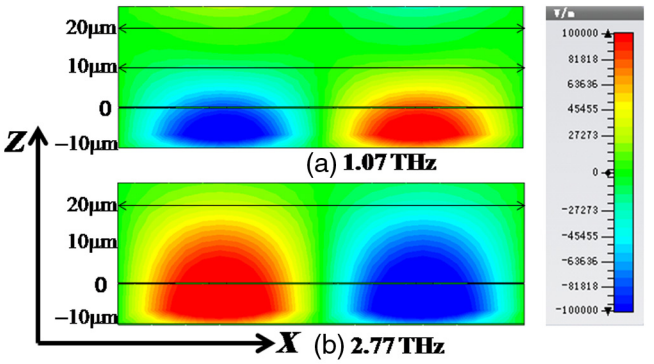

Fig. 7 Electric field distribution in the *z*-direction of THz dual-band absorber at (a) 1.07 and (b) 2.77 THz.

Additionally, the change in amplitude absorption was achieved for the resonance f_2.

In Fig. 6(b), the relative frequency shift (RFS) in the refractive index for the resonances f_1 and f_2 was also studied, the RFS was defined as RFS $= \frac{(f_n - f_{\text{Ref}})}{f_{\text{Ref}}} \times 100\%$, where f_{Ref} is the resonance frequency of the flexible absorber without any analyte and f_n is the resonance frequency of the flexible absorber with analyte refractive index (n). The frequency sensitivity is defined as $\mathrm{d}f/\mathrm{d}n$, the slope of linear fitting function, where $\mathrm{d}f$ is the change of resonance frequency and $\mathrm{d}n$ is the change of the refractive index. The sensitivity (S) is 31.2% refractive index units $(\text{RIU})^{-1}$ for the resonance f_2 and 13.7% RIU^{-1} for the resonance f_1. The amplitude absorption and the frequency shift with the different refractive indices were also characterized for the resonance f_2 [Fig. 6(c)], the fitting functions for the amplitude absorption are described by $y_4 = 1.0827 - 0.0071e(-\frac{n}{0.4315})$ and $y_5 = 553 * n - 586$, respectively. Therefore, this designed absorber can be applied to identify the unknown materials by the amplitude absorption change and the frequency shift. By applying the method, higher accuracy biosensor can be achieved as privileges over conventional through the frequency shift or the amplitude modulation. To quantitatively characterize the absorber sensor, we also calculated the FOM. The FOM was defined as FOM $= S \times Q$, where S is the sensitivity of the THz flexible absorber and Q is the quality factor of the resonance f. The FOM was 17.2 for the resonance f_2 and 1.2 for the resonance f_1. The FOM value of the high-order resonance is 7.5 times than that of the recent results.[14]

From the simulation analytical results, we determined that the designed THz dual-band metamaterial absorber was capable of sensing the solid analyte. From Fig. 5(c), we also noted that the frequency shift became saturated at analyte thicknesses over 10 and 25 μm of the resonances f_1 and f_2, respectively, and no further significant frequency shift was observed.

To qualitatively explain the properties, we simulated the electric field distribution in the $x-z$ plane for the THz absorber (Fig. 7). The electric field fell off quickly away from the metamaterial absorber layer and can be neglected above 10 μm for the resonance f_1 and 30 μm for the resonance f_2. According to a previous report,[25] the equivalent capacitance c_{eff} can be expressed as

$$c_{\text{eff}} = \frac{Q_{\text{eff}}}{U_{\text{eff}}} = \frac{\int_V \varepsilon_0 \varepsilon_r \vec{E}.\mathrm{d}\vec{A}}{\int_{p_1}^{p_2} \vec{E}.\vec{x}\mathrm{d}x} \infty \int \varepsilon_r(z)\vec{E}(z).\vec{x}\mathrm{d}z. \quad (1)$$

Thus, the equivalent capacitance changes slightly with a further increase in coating thickness, and the frequency changes tend to be saturated.

2.3 *Aqueous Solution Sensing*

However, metamaterials for aqueous solution sensing are rarely reported; thus, we further characterized the designed THz absorber sensor for aqueous solutions. Figure 8(a) displays the simulated absorption for aqueous solutions of ethanol. The thickness of the aqueous layer was 15 μm. The red frequency shifts of the resonance f_1 for the dielectric constants of $2.6 + 0.9i$, $2.8 + 1.1i$, and $3.2 + 1.3i$ were 124, 142, and 172 GHz, respectively.[26] The frequency shifts of 140, 152, and 211 GHz of the dielectric constants for the resonance f_2 were higher than those of frequency shift f_1.

However, the resonance intensity f_2 becomes weaker with an increase in the dielectric constant of the ethanol–water mixture and the amplitude absorption of the resonance f_1 increased. From the above analytical results, we know that the resonance f_2 originated from the interactions of adjacent

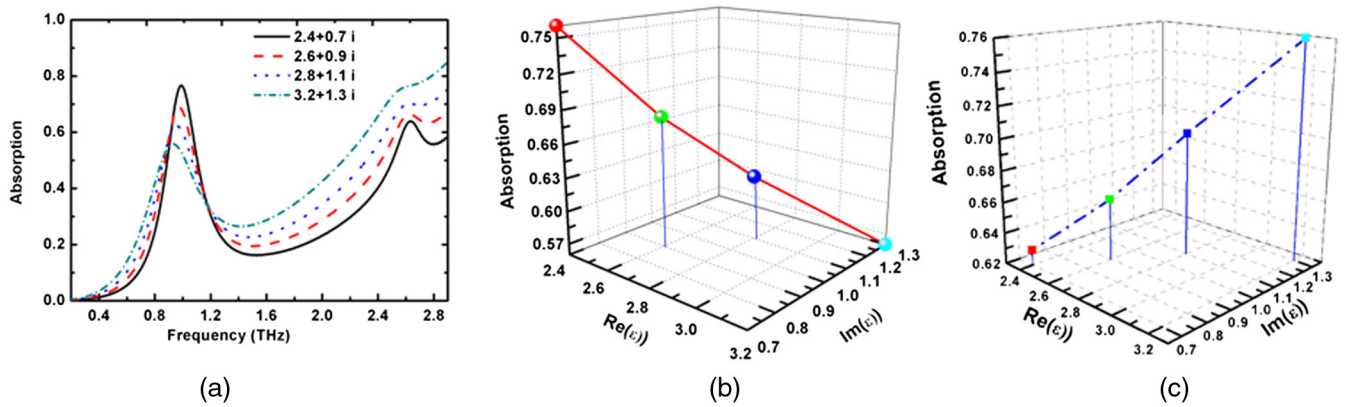

Fig. 8 (a) Simulated THz absorber spectra of the ethanol–water mixture in different concentrations. (b) Simulated absorption as a function of the dielectric constant of the ethanol–water mixture at the resonance f_1. (c) Simulated absorption as a function of the dielectric constant of the ethanol–water mixture at the resonance f_2.

unit cells, and it has more sensitivity to the variation of the dielectric constant. Compared to solid analyte, aqueous solution has greater loss for larger imaginary part for the dielectric constants result in the becoming weak of resonance and increasing absorption f_2. The absorption amplitude and frequency shift of the resonance f_2 are different from that of the resonance f_1 varying with the dielectric constant of the aqueous solution.

The dielectric constant dependence of the amplitude absorption for the resonances f_1 and f_2 was also studied as shown in Figs. 8(b) and 8(c). Obviously, the amplitude absorption for the resonances f_1 and f_2 reduced linearly when increasing the dielectric constant of the ethanol–water mixture.

Therefore, the proposed metamaterial absorber also provided an effective method to probe the molecular or ionic concentrations and did not require the penetration of a water layer.

3 Discussion

We demonstrated a flexible THz dual-band metamaterial absorber, which exhibited sensitivity in sensing solid analyte and aqueous solutions through the frequency shift and the amplitude absorption. For the solid analyte, a linear relation was observed between the thickness of the analyte and the amplitude absorption for the high-order resonance f_2, and the exponential and line relation were obtained among the refractive index, the amplitude absorption, and the frequency shift of the high-order resonance f_2, respectively. For the aqueous solution, a linear relation was also achieved between the amplitude absorption and dielectric constant of the ethanol–water mixture of the resonance f_1. In the detection techniques for sensing materials, frequency shift at two resonances can enhance accuracy. The proposed THz absorber can be applied for highly accurate and sensitive monitoring of biomolecular chemical aqueous biosystems and ecological water systems in the future.

Acknowledgments

X.Y. and L.J.L. performed numerical simulations and prepared the samples. All the authors wrote the paper. J.Q.Y. directed the research. The authors declare no competing financial interests. The research was supported by the National Natural Science Foundation (No. 61675147), the China Postdoctoral Science Foundation (No. 2015M571263), the Programe of Independent Innovation and Achievement Transformation Plan for Zaozhuang (No. 2016GH19), Science and Technology Program of Zaozhuang (No. 2016GX31), and Zaozhuang Engineering Research Center of Terahertz and the Doctoral Foundation.

References

1. Y. Rivenson et al., "Overview of compressive sensing techniques applied in holography," *Appl. Opt.* **52**(1), A423 (2013).
2. N. Kida et al., "Characteristic effect of an anticancer dinuclear platinum (II) complex on the higher-order structure of DNA," *J. Biolog. Inorg. Chem.* **15**(5), 701–707 (2010).
3. V. Cassina et al., "Atomic force microscopy study of DNA conformation in the presence of drugs," *Europ. Biophys. J.* **40**(1), 59–68 (2011).
4. Q. Zhu et al., "Ultrasensitive simultaneous detection of four biomarkers based on hybridization chain reaction and biotin–streptavidin signal amplification strategy," *Biosens. Bioelectron.* **68**(15), 42–48 (2015).
5. E. F. Aziz et al., "Interaction between liquid water and hydroxide revealed by core-hole de-excitation," *Nature* **455**, 89–91 (2008).
6. K. J. Tielrooij et al., "Cooperativity in ion hydration," *Science* **328**, 1006–1009 (2010).
7. X. X. Han et al., "Label-free indirect immunoassay using an avidin-induced surface-enhanced Raman scattering substrate," *Small* **7**, 316–320 (2011).
8. X. J. Wu et al., "Label-free monitoring of interaction between DNA and oxaliplatin in aqueous solution by terahertz spectroscopy," *Appl. Phys. Lett.* **101**, 033704 (2012).
9. K. He et al., "Y-shaped probe for convenient and label-free detection of microRNA-21 in vitro," *Anal. Biochem.* **499**, 8 (2016).
10. S. Ebbinghaus et al., "Protein sequence-and pH-dependent hydration probed by terahertz spectroscopy," *J. Am. Chem. Soc.* **130**(8), 2374–2375 (2008).
11. P. U. Jepsen et al., "Terahertz spectroscopy and imaging–modern techniques and applications," *Laser Photonics Rev.* **5**, 124–166 (2011).
12. J. S. Melinger et al., "Temperature dependent characterization of terahertz vibrations of explosives and related threat materials," *Opt. Exp.* **18**(26), 27238 (2010).
13. E. Arik et al., "Dielectric properties of ethanol and gasoline mixtures by terahertz spectroscopy and an effective method for determination of ethanol content of gasoline," *J. Phys. Chem. A* **118**(17), 3081–3089 (2014).
14. L. Q. Cong et al., "Experimental demonstration of ultrasensitive sensing with terahertz metamaterial absorbers: a comparison with the metasurfaces," *Appl. Phys. Lett.* **106**, 031107 (2015).
15. R. J. Singh et al., "Ultrasensitive terahertz sensing with high-Q Fano resonances in metasurface," *Appl. Phys. Lett.* **105**, 171101 (2014).
16. B. X. Wang et al., "A novel dual-band terahertz metamaterial ansorber for a sensor application," *J. Appl. Phys.* **117**, 14504 (2015).
17. X. Wu et al., "Sensing self-assembled alkanethiols by differential transmission interrogation with terahertz metamaterials," *Appl. Opt.* **52**(20), 4877 (2013).
18. L. Q. Cong et al., "Fano resonances in terahertz metasurfaces: a figure of merit optimization," *Adv. Opt. Mater.* **3**, 1537–1543 (2015).
19. H. Tao et al., "Silk-based conformal, adhesive, edible food sensors," *Adv. Mater.* **24**, 1067–1072 (2012).
20. L. J. Xie et al., "Extraordinary sensitivity enhancement by metasurface in terahertz detection of antibiotics," *Sci. Rep.* **5**, 1038 (2015).
21. D. Kaikai et al., "Wavelength and thermal distribution selectable microbolometers based on metamaterial absorbers," *IEEE Photon. J.* **7**, 6800908 (2014).
22. B. Kearney et al., "Al/SiOx/Al single and multiband metamaterial absorbers for terahertz sensor applications," *Opt. Eng.* **52**(1), 013801 (2013).
23. W. X. Yu et al., "Meta-microwindmill structure with multiple absorption peaks for the detection of ketamine and amphetamine type stimulants in terahertz domain," *Opt. Mater. Exp.* **4**, 234 (2014).
24. X. J. Wu et al., "Alkanethiol-functionlized terahertz metamaterial as label-free, highly-sensitive and specific biosensor," *Biosens. Bioelectron.* **42**, 626–631 (2013).
25. B. Reinhard et al., "Metamaterial near-field sensor for deep-subwavelength thickness measurements and sensitive refractometry in the terahertz frequency range," *Appl. Phys. Lett.* **100**, 221101 (2012).
26. X. J. Wu et al., "Self-referenced sensing based on terahertz metamaterial for aqueous solutions," *Appl. Phys. Lett.* **102**, 151109 (2013).

Xin Yan is doctoral student at the University of Tianjin. He received his BS degree in physics from Yili Normal University in 2002 and his MS degree in optics from Zhengzhou University in 2008. He is the author of more than 30 journal papers. His current research interests include terahertz devices, metamaterials, and photonic crystals.

Lan-Ju Liang received her BS degree in physics from Yili Normal University in 2002, her MS degree in physical electronics from QuFu Normal University in 2005, and her PhD in electromagnetic field and microwave technology from Nanjing University in 2014. She is post doctoral at the University of Tianjin. Her current research interests include terahertz devices and metamaterials.

Xin Ding received his PhD in physical electronics from Tianjin University in 2000. He is a professor with the College of Precision Instrument and Optoelectronics Engineering, Tianjin University, Tianjin, China. His current research interests include terahertz devices, metamaterials, and lasers.

Jian-Quan Yao received his MS degree in optics from Tianjin University in 1965. He is currently an academician with the Chinese Academy of Sciences, Beijing, China. He is a professor with the College of Precision Instrument and Optoelectronics Engineering, Tianjin University, Tianjin, China. His current research interests include terahertz source, terahertz device, metamaterials, and lasers.